

Compensation for Illumination Changes on Whisk-broom Hyperspectral Imaging

TAKEHIRO OGAWA^{1,a)} TAKUYA FUNATOMI^{1,b)} KENICHIRO TANAKA¹ HIROYUKI KUBO¹
YASUHIRO MUKAIGAWA¹

Abstract

We propose a method of compensating for the temporal variation in environmental illumination in whisk-broom hyperspectral imaging. In addition to the standard two-dimensional scan, we propose the execution of an extra one-dimensional scan orthogonal to the scanline as a reference for the compensation. Our method uses a low-dimensional structure in the spectral property of illumination to robustly compensate for illumination changes. We quantitatively evaluate the compensation methods in an experiment conducted under controlled illumination and present the results of a field experiment.

1. Introduction

In the field of computer vision, remarkable advances in camera technology allow robots to better understand a scene visually than humans. Spectral data recorded by specialized cameras are superior to RGB images captured by the human eye in terms of sensitive detection in, for example, chemistry and art conservation. Examples of such application are the monitoring of agricultural crops, soil, and forests, biomedical engineering, biometrics, and facial recognition in the field of computer vision.

Although some studies [1], [3], [4], [5] have inferred spectral images from RGB images, there are still demands for measuring spectral images accurately. As one device that meets such demands, a *whisk-broom* sensor comprises a high-resolution spectrometer and a mechanical scanning system as shown in Fig. 1. The spectrometer measures a spectral distribution at a single point and the mechanical system thus scans a scene spatially to compose an image row by row from top to bottom, and from left to right within each row. Blue arrows in Fig. 1 (b) illustrate the scanning.

While such a system allows the capture of a hyperspectral image with thousands of spectral channels, it takes a long time (*e.g.*, a few hours) to scan a whole scene. Any temporal variation in the environmental illumination is therefore a problem, especially when the system captures light passively.

The present paper proposes a method of compensating for changes in environmental illumination using the high operability of the scanner and low-dimensional structure in the spec-

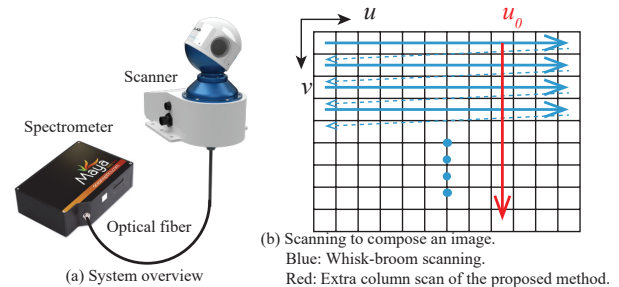


Fig. 1 Whisk-broom imaging system. (a) Overview of the system overview developed in this study. (b) Blue arrows illustrate the whisk-broom scanning in compose an image. Red arrow illustrates the extra 1D scan conducted in the proposed method.

tral factor of illumination. We specifically introduce an extra one-dimensional (1D) scan that is perpendicular to the scan line and regularize the spectral volume using the low-rank nature of the spectrum [6]. Through low-rank optimization, the proposed method is robust against noisy measurements. The effectiveness is confirmed in a field experiment and laboratory experiments.

The contribution of this paper is that by combining the advantages of whisk-broom measurement and low-rank optimization, a hyperspectral volume with high spatial and spectral resolution is now available even under variable illumination. The specific achievements of the paper are as follows.

- An extra 1D scan is proposed in addition to the standard two-dimensional (2D) scan, using the high operability of the whisk-broom sensor.
- The low-dimensional structure in high-dimensional spectral data is utilized to improve the performance of compensation.
- A problem of instability is clarified through experiments conducted in a controlled environment and in the field.

2. Mathematical model

A hyperspectral image is commonly called a *spectral cube* because it has many channels along the spectrum. The present paper also considers a temporal factor of illumination change. We therefore denote by $S(u, v, t, \lambda)$ a spectral cube with the spatial coordinate (u, v) , time t , and spectrum λ .

Suppose that there are temporal changes in the environmental illumination of a static scene. The spectral cube can be decomposed as

$$S(u, v, t, \lambda) = L(t, \lambda)R(u, v, \lambda), \quad (1)$$

where $L(t, \lambda)$ is the environmental illumination, which is spa-

¹ Nara Institute of Science and Technology

^{a)} ogawa.takehiro.ol1@is.naist.jp

^{b)} funatomi@is.naist.jp

tially uniform, and $R(u, v, \lambda)$ is the reflectance/transmittance of the scene, which is temporally invariant.

Here, our goal is to recover a spectral cube under a constant illumination $L_r(\lambda) = L(t_r, \lambda)$ at a time t_r , which is mathematically defined as

$$S_r(u, v, \lambda) = L_r(\lambda)R(u, v, \lambda). \quad (2)$$

If a reflectance or transmittance standard is captured at a pixel, $R(u, v, \lambda)$ is easily recovered if $S_r(u, v, \lambda)$ is given.

In whisk-broom imaging, the scanning consists of multiple row scans as presented in Fig. 1 (b). We assume that illumination changes are negligible in each row. Accordingly, the captured spectral cube is formulated as

$$S_{wb}(u, v, t(v), \lambda) = L(t(v), \lambda)R(u, v, \lambda), \quad (3)$$

where the time of the scan is represented as a function of the row of the image.

3. Compensation for illumination changes

3.1 Extra 1D scan in a minute for compensation

Each row of S_{wb} is independently affected by changes in temporal illumination; however, there is no clue with which to compensate for changes along a column. We therefore execute an extra single-column scan, which corresponds to the red arrow in Fig. 1 (b), in addition to the imaging scan that comprises multiple row scans. The illumination changes can also be negligible in the column as well as in each row. Accordingly, the extra 1D scan is formulated as

$$S_r(u_r, v, \lambda) = L_r(\lambda)R(u_r, v, \lambda), \quad (4)$$

where u_r represents the scanned column. We propose a method of compensating for temporally varying illumination in $S_{wb}(u, v, t(v), \lambda)$ to be fit to the spectral cube $S_r(u, v, \lambda) = S(u, v, t_r, \lambda)$, where t_r is the time when the extra scan is conducted.

3.2 A naïve method for compensation

Because any row in the image and the column of the extra scan share one pixel, which corresponds to any of the intersections of the blue arrows and the red arrow in Fig. 1 (b), we can extract the spectral factor of the illumination change at the pixel. By comparing the corresponding pixel in S_{wb} and S_r , we obtain a coefficient $C_n(v, \lambda)$ of illumination change for each spectrum:

$$C_n(v, \lambda) = \frac{S_r(u_r, v, \lambda)}{S_{wb}(u_r, v, t(v), \lambda)} = \frac{L_r(\lambda)}{L(t(v), \lambda)} \quad (5)$$

By multiplying the coefficients with the spectrum at other pixels in the row, we estimate the spectra of the row under the illumination at the moment when S_r is captured. As a naïve method, illumination changes are compensated for according to

$$S_n(u, v, \lambda) = C_n(v, \lambda)S_{wb}(u, v, t(v), \lambda), \quad (6)$$

where $S_n(u, v, \lambda)$ is a spectral cube compensated using the naïve method.

The naïve method will work well if the shared pixel has a uniform spectral feature, such as a reflectance/transmittance standard. However, if the pixel captures a colored object, some spectra could have low intensity in both S_{wb} and S_r . As a result, the coefficients of such spectra become unstable because both the numerator and denominator are small values and errors are dominant.

When another pixel in the row captures a target with a different spectral feature, the spectral distribution can be distorted at the spectra owing to the unstable coefficients. Accordingly, the corrected spectra has large error at such a pixel.

3.3 Extracting a low-dimensional spectral factor of illumination

We introduce a constraint to the coefficients to suppress the effects of unstable coefficients. It is naturally assumed that illumination has a low-dimensional spectral structure [6]. We thus approximate the spectral distribution of illumination using a small number of bases:

$$L(t, \lambda) \simeq \sum_k w_k(t)l_k(\lambda), \quad (7)$$

where $l_k(\lambda)$ and $w_k(t)$ denote the spectral bases and their weights. $L_r(\lambda)$ can be treated as a constant and we thus approximate Eq. (5) as

$$C_n(v, \lambda) \simeq \sum_k w_k(t(v)) \frac{L_r(\lambda)}{l_k(t(v), \lambda)} = \sum_k w'_k(v)l'_k(\lambda). \quad (8)$$

Note that we can represent $\frac{1}{C_n(v, \lambda)}$ as the linear combination of bases more precisely than $C_n(v, \lambda)$. However, it turns out that using $\frac{1}{C_n(v, \lambda)}$ leads to numerical instability in the compensation calculation of Eq. (6) in practice. We therefore approximate $\frac{1}{C_n(v, \lambda)}$ using other bases $l'_k(\lambda)$ even though this is not mathematically ideal.

$C_n(v, \lambda)$ is now ideally approximated as $\sum_k w'_k(v)l'_k(\lambda)$; however, it may have outliers where $S(u_r, v, \lambda)$ is dominated by error. In practice, therefore, $C_n(v, \lambda)$ needs to be treated as a superposition of a low-rank coefficients matrix $C_l(v, \lambda) = \sum_k w'_k(v)l'_k(\lambda)$ with rank k and a sparse component of outliers expressed as C_s :

$$C_n(v, \lambda) = C_l(v, \lambda) + C_s. \quad (9)$$

We adopt robust principal component analysis [2] to extract the low-dimensional structure, which is achieved by solving

$$\begin{aligned} \min_{C_l(v, \lambda), C_s} & \|C_l(v, \lambda)\|_* + \mu \|C_s\|_1 \\ \text{subject to} & C_n(v, \lambda) = C_l(v, \lambda) + C_s, \end{aligned} \quad (10)$$

where $\|\cdot\|_*$ denotes the nuclear norm, $\|\cdot\|_1$ refers to the l_1 -norm that serves as convex relaxations of rank and sparsity, and μ is a regularization parameter, which is set as 10^{-6} here.

This allows us to decompose $C_n(v, \lambda)$ into low-rank coefficients $C_l(v, \lambda)$ and a sparse outlier matrix C_s . Using the low dimensionality in $C_l(v, \lambda)$, the unstable coefficients can be exactly recovered from the coefficients of spectra with sufficient intensity. The recovered coefficients are expected to effectively

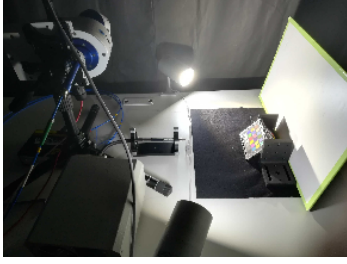


Fig. 2 Setting for experiments. A variable halogen light and two LEDs are set to illuminate a color chart.

compensate for illumination changes at other pixels.

In addition to Eq. (6), the compensation for the illumination changes is

$$S_{es}(u, v, \lambda) = C_l(v, \lambda)S_{wb}(u, v, t(v), \lambda), \quad (11)$$

where $S_{es}(u, v, \lambda)$ is the compensated spectral cube by the proposed method.

4. Experiments

We developed an imaging system comprising a single-point spectrometer and scanner. Figure 1 (a) illustrates the composition of the system. The spectrometer is a Maya2000 Pro (Ocean Optics, Inc.), which covers the wavelength range of 200–1100 nm with a resolution of about 0.5 nm and outputs 2068 bands. The scanner is a RobotEye REHS25 (Ocular Robotics Ltd.) that scans with spatial resolution up to 0.01° through 360° in the pitch direction and 70° in the yaw direction. These devices are connected using an optical fiber.

4.1 Laboratory Experiment

We first evaluated the compensation methods under a controlled environment in the laboratory as shown in Fig. 2. We prepared a variable halogen light and two light-emitting diodes (LEDs). We imitated a measurement under illumination changes by temporally changing the intensity of the halogen light by hand. We captured a hyperspectral image with constant illumination where only the LEDs are on. The image is considered the ground truth $S_{gt}(u, v, \lambda)$ and one of the columns is used as an extra 1D scan $S_r(u_r, v, \lambda)$ for the compensation. We also captured a hyperspectral image $S_{wb}(u, v, t(v), \lambda)$, which comprised multiple row scans, with illumination changes. We evaluate the methods by comparing the compensated results with the ground truth.

We use the mean of the absolute error in wavelength as our metric with which to verify the quantitative accuracy of the compensation for illumination changes:

$$err(u, v) = \frac{1}{|\Lambda|} \sum_{\lambda \in \Lambda} \|(S(u, v, \lambda) - S_{gt}(u, v, \lambda))\|, \quad (12)$$

where $|\Lambda|$ is the number of bands at the pixel.

We present RGB images by extracting three channels ($\lambda = 635.8, 546.0, 435.8$ nm) of the results of compensation for the illumination changes in Fig. 3. Both compensated results are much closer to the ground truth than the input image captured under temporally variable illumination.

Figure 4 presents an error map of the results of the naïve and

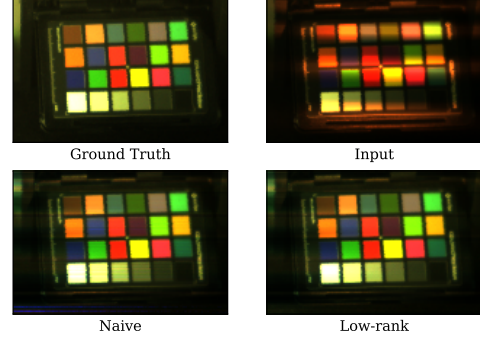


Fig. 3 The results of the experiment in the lab. The top row consists of captured images under constant and temporally variable illumination. The bottom row consists of the compensated results using the naïve and the proposed methods.

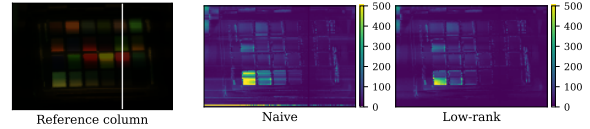


Fig. 4 Error map of the results of the naïve and the proposed methods relative to the ground truth.

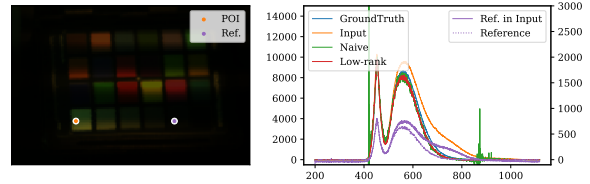


Fig. 5 Spectral distributions at a POI and corresponding reference point. Both compensated results are close to the ground truth; however, the result of the naïve method has large error for some spectra.

proposed methods relative to the ground truth and illustrates the column u_r in the image used for compensation. The figure shows that the error when using the naïve method is greater than that when using the proposed method. Figure 5 presents the spectral distributions at a point of interest (POI) and the corresponding reference point. Both compensated results are close to the ground truth; however, the result of the naïve method has large errors for some spectra, such as $\lambda = 419\text{--}424$ and $868\text{--}875$ nm. We also see that these spectra of the reference point have a weak signal. Meanwhile, the proposed method successfully recovered these spectra and others thanks to the low-rank and sparse decomposition.

The set of results presented above is only an example of the compensation and the results strongly depend on the column used as the reference. We therefore investigated the robustness of the methods against the selection of the reference column. Figure 6 shows the performance of the methods with respect to the selection of the reference column. The performance is evaluated as the mean error over the whole image. The performance of the proposed method is consistently better than that of the naïve method, which has especially worse performance when the reference column contains dark parts. This analysis demonstrates the robustness of the proposed method.

We captured sunlight transmitted through stained glass in a cathedral using the proposed system. Even though RobotEye allows scanning as fast as 25 points/s, its use was time consuming

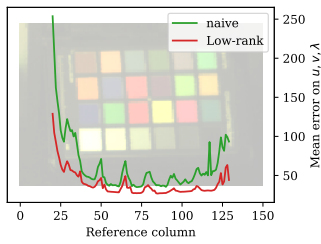


Fig. 6 Mean error in the results of the naïve and proposed methods versus the selection of the reference column. The proposed method with the low-rank assumption is always more accurate than the naïve method, which has especially worse performance when the reference column contains black parts.

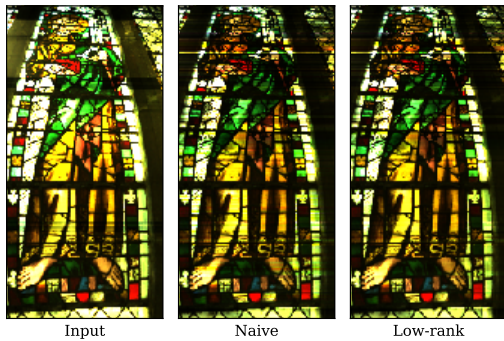


Fig. 7 Captured image and compensated results of the field experiment.

in capturing a hyperspectral image with a certain spatial resolution. As an example, it takes about 1 hour to capture an image having a resolution of 300×300 . Because this measurement was executed under natural sunlight, it was impossible to escape temporal changes in sunlight intensity due to natural processes, such as the movement of clouds and the rotation of the Earth. We obtained multiple scans for the stained glass as follows.

- (1) 2D capture with a resolution of 400×200 , taking 3217.7 s.
- (2) 1D capture of 400×1 orthogonal to the scanline direction. The extra 1D capture took 15.6 s and was negligibly affected by changes in sunlight.

As well as in Sec. 4.1, we applied both methods to the hyperspectral image of a stained-glass. Figure 7 shows the RGB images of the input and the compensated results. Figure 8 also shows the spectral distributions at a point of interest (POI) and the corresponding reference point. Although we cannot evaluate the results quantitatively because there is no ground truth, the spectral distribution of the naïve method has unnaturally large values, such as an outlier, for some spectra as in the laboratory experiment, and the spectral distribution itself seems slightly erroneous relative to the distribution obtained using the proposed method. This infers that the proposed method achieves better compensation than the naïve method.

5. Conclusion

We proposed a method of compensating for the temporal variation in environmental illumination in whisk-broom hyperspectral imaging. The method assumes that illumination changes are negligible in a one-line scan and compensates for changes among the rows of a hyperspectral image. In addition to the standard 2D scan, we executed an extra 1D scan orthogonal to the scanline as a reference for the compensation. We clarified that the coefficients

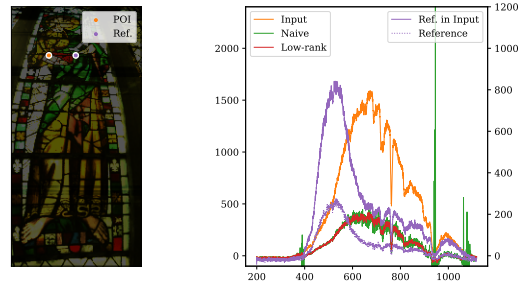


Fig. 8 Spectral distributions at a POI and corresponding reference point. The results of the naïve method have an unnatural spectral distribution.

of the compensation directly estimated from the reference can be unstable depending on the measured target but this can be overcome using a low-dimensional structure in the spectral property of illumination. We quantitatively evaluated the compensation methods in an experiment conducted under controlled illumination and presented the results of a field experiment.

Recent hyperspectral cameras adopt another mechanism called the *push-broom* mechanism, where a scene is scanned in a series of lines. This mechanism uses a 2D array of photodetectors to scan both spatially and spectrally, dramatically reducing the scan time. The assumptions of the proposed method are well suited to the push-broom system; however, there remains the issue of how to realize the extra column scan in the mechanism. This application is left as promising future work.

Acknowledgements

This study is partly supported by JSPS and MAEDI under the Japan–France Integrated Action Program (SAKURA) and Japan Science and Technology Agency CREST Grant Number JPMJCR1764. We acknowledge Prof. El Mustapha Mouadib and Prof. Guillaume Caron (University of Picardie Jules Verne), Prof. Cédric Demonceaux (University of Burgundy), and Dr. Nicolas Ragot (ESIGELEC) for their support in executing the experiments in Amiens Cathedral, France. We acknowledge Prof. Yasuyuki Matsushita and Ms. Tomoka Takemura (Osaka University) for their support in applying robust principal component analysis.

References

- [1] Baek, S.-H., Kim, I., Gutierrez, D. and Kim, M. H.: Compact Single-Shot Hyperspectral Imaging Using a Prism, *ACM Transactions on Graphics(Proc. SIGGRAPH Asia 2017)*, Vol. 36, No. 6, pp. 217:1–12 (2017).
- [2] Candès, E. J., Li, X., Ma, Y. and Wright, J.: Robust Principal Component Analysis?, *J. ACM*, Vol. 58, No. 3, pp. 11:1–11:37 (2011).
- [3] Chi, C., Yoo, H. and Ben-Ezra, M.: Multi-Spectral Imaging by Optimized Wide Band Illumination, *International Journal of Computer Vision*, Vol. 86, No. 2, p. 140 (2008).
- [4] Choi, I., Jeon, D. S., Nam, G., Gutierrez, D. and Kim, M. H.: High-Quality Hyperspectral Reconstruction Using a Spectral Prior, *ACM Transactions on Graphics(Proc. SIGGRAPH Asia 2017)*, Vol. 36, No. 6, pp. 218:1–13 (2017).
- [5] Jia, Y., Zheng, Y., Gu, L., Subpa-Asa, A., Lam, A., Sato, Y. and Sato, I.: From RGB to Spectrum for Natural Scenes via Manifold-Based Mapping, *2017 IEEE International Conference on Computer Vision(ICCV)*, pp. 4715–4723 (2017).
- [6] Judd, D. B., MacAdam, D. L., Wyszecki, G., Budde, H. W., Condit, H. R., Henderson, S. T. and Simonds, J. L.: Spectral Distribution of Typical Daylight as a Function of Correlated Color Temperature, *J. Opt. Soc. Am.*, Vol. 54, No. 8, pp. 1031–1040 (1964).